The size of an ERS SAR single-look pixel on the ground is 4 m in azimuth and 20 m in range. This technique is similar to the approach developed by R. E. Crippen [*Episodes* **15**, 56 (1992)] with visible satellite images (SPOT).
15. At 35°N latitude on descending orbit passes, the incidence angle difference between lines of sight of adjacent orbits varies from 4.6° to 4.9° between the far range (western edge) and the near range (eastern edge) of the area of swath overlap (*13*).
16. The line-of-sight projection of a displacement vector (e, n, u) in the local east, north, up reference frame is $r = [e\cos(\alpha) - n\sin(\alpha)]\sin(i) + u\cos(i)$, where α is the angle between the azimuthal direction of the displacement vector and the direction perpendicular to the satellite track, and i is the incidence angle (*13*). For horizontal displacement fields ($u = 0$), the observed cross-track component of the displacement vector is $r/\sin(i)$ and is independent of the incidence angle.
17. The source time function of the earthquake depicts a similar bimodal shape with a main pulse moment of $\sim 1.5 \times 10^{20}$ Nm in the first 30 s followed by a smaller pulse of 10 s [University of Michigan Web site: www.geo.lsa.umich.edu/SeismoObs/STF.html (1997); A. Velasco, personal communication (1998)].
18. Seismic and radar data indicate that only one fault was involved in the earthquake. Shear stress across the fault must be continuous (equilibrium conditions). Observed displacement asymmetry indicates that strain is not continuous across the fault. Thus, elastic properties must be different between the two sides of the fault. The particular form of asymmetry observed in the displacement curves (Fig. 4B) suggests that elastic properties are correlated with volume strain and not related to crustal heterogeneities along the rupture.
19. W. R. Delameter, G. Herrmann, D. M. Barnett, *J. Appl. Mech.* **47**, 74 (1975); E. R. Ivins and G. A. Lyzenga, *Philos. Trans. R. Soc. London Ser. A* **318**, 285 (1986).
20. F. Saucier, thesis, University of Oregon (1991).
21. This approach is akin to a first-order perturbation approach with respect to a linear model because we implicitly assume that the locations of compressional and tensile volumes are unchanged by nonlinearity.
22. Given the symmetry of the fault geometry and slip distribution of the model, the along-strike distribution of the fault-parallel, horizontal component of the displacement vector is symmetric with respect to the auxiliary plane and the distribution of the vertical component is antisymmetric. The line-of-sight projection of the vector combines all components of the displacement vector (*16*) and thus depicts the antisymmetry of its vertical component with respect to the auxiliary plane.
23. R. Muir-Wood and G. C. P. King, *J. Geophys. Res.* **98**, 22035 (1993).
24. A. Nur and J. R. Booker, *Science* **175**, 885 (1972); D. L. Anderson and J. H. Whitecomb, *J. Geophys. Res.* **80**, 1497 (1975); K. W. Hudnut, L. Seeber, J. Pacheo, *Geophys. Res. Lett.* **16**, 199 (1989); C. H. Scholz, *Geology* **2**, 551 (1974); J. B. Rundle and W. Thatcher, *Bull. Seismol. Soc. Am.* **70**, 1869 (1980); G. Peltzer, P. Rosen, F. Rogez, K. Hudnut, *Science* **273**, 1202 (1996).
25. A drop of seismic velocities at depths shallower than 3 to 5 km is observed in many places [P. Reasenberg and W. L. Ellsworth, *J. Geophys. Res.* **87**, 10637 (1982); A. W. Walter and W. D. Mooney, *Bull. Seismol. Soc. Am.* **72**, 1567 (1982); L. D. Dietz and W. L. Ellsworth, *Geophys. Res. Lett.* **17**, 1417 (1990); C. Dorbath, D. Oppenheimer, F. Amelung, G. King, *J. Geophys. Res.* **101**, 27917 (1996)] and is generally attributed to the presence of open cracks not saturated with fluids in the shallow crust.
26. D. Massonnet *et al.*, *Nature* **364**, 138 (1993).
27. At longitude E87.17° and latitude N34.60° the interferogram shows a double lobe, ~10-km-long pattern, with a maximum range change corresponding to ~10 cm of surface uplift and bounded to the north by an east-west, ~8-km-long line of phase discontinuity. We interpret this feature as the surface displacement field associated with a shallow earthquake having occurred between 19 August and 2 December 1997. The observed displacement and phase discontinuity suggest that the event has left-lateral and thrust components and a fault plane steeply dipping to the south (F. Crampé and G. Peltzer, in preparation). We note, however, that the geographic location of this feature is 30 km away from the nearest aftershock epicenter determined by the NEIC during the same period. This may be due either to large errors in the localization of aftershocks or to the fact that this shallow event occurred during the propagation of the main rupture, making its seismic record indistinguishable from that of the main event.

28. We thank P. Bernard, F. Cornet, E. Ivins, and H. Kanamori for fruitful discussions; P. Lundgren for help with the modeling; and two anonymous reviewers for constructive comments. ERS data were provided by the European Space Agency. Work for this study was done at the Jet Propulsion Laboratory, California Institute of Technology, under contract with NASA.

7 June 1999; accepted 11 August 1999

Measurements of Past Ice Sheet Elevations in Interior West Antarctica

Robert P. Ackert Jr.,[1]* David J. Barclay,[3] Harold W. Borns Jr.,[4] Parker E. Calkin,[6] Mark D. Kurz,[2] James L. Fastook,[5] Eric J. Steig[7]

A lateral moraine band on Mount Waesche, a volcanic nunatak in Marie Byrd Land, provides estimates of past ice sheet surface elevations in West Antarctica. Helium-3 and chlorine-36 surface exposure ages indicate that the proximal part of the moraine, up to 45 meters above the present ice surface, was deposited about 10,000 years ago, substantially later than the maximum ice extent in the Ross Embayment. The upper distal part of the moraine may record multiple earlier ice sheet high stands. A nonequilibrium ice sheet model predicts a delay of several thousand years in maximum ice levels at Mount Waesche relative to the maximum ice extent in the Ross Sea. The glacial geologic evidence, coupled with the ice sheet model, indicates that the contribution of the Ross Sea sector of the West Antarctic Ice Sheet to Holocene sea level rise was only about 3 meters. These results eliminate West Antarctic ice as the principle source of the large meltwater pulse during the early Holocene.

Knowledge of the past configurations and behavior of the West Antarctic Ice Sheet (WAIS) is necessary to calibrate glaciological models that attempt to predict future responses of the ice sheet and to quantify the contribution of the Antarctic ice sheets to eustatic sea level rise during the last deglaciation. Outlet glaciers in the Transantarctic Mountains were once dammed by thick grounded ice in the Ross Embayment, where only a floating ice shelf occurs today (*1*). In the McMurdo Sound region, ^{14}C and surface exposure ages on drift deposited by ice grounded in the Ross Sea date to the last glacial maximum (LGM) (*2*). Geophysical mapping of the Ross Sea floor (*3*) and ^{14}C ages on sediments overlying tills (*4*) demonstrate that grounded ice extended to near the continental shelf break at the LGM, over 1000 km beyond the present grounding line.

In contrast to its extent, direct evidence for the interior elevation of the WAIS has been quite uncertain. An ice sheet model constrained by the evidence from the Ross Embayment, trimlines in the Ellsworth Mountains, and striations on the Hobbs coast suggests that ice sheet domes in West Antarctica were 450 to 600 m higher during the LGM (*5*). However, the age of the trimlines and striations is uncertain, and this reconstruction may overestimate interior elevations (*5*). Total gas content from the Byrd ice core, which is largely a function of past atmospheric pressure (elevation of the site) (*6*), has been interpreted as indicating that ice elevations were ~200 m lower (*7*) and 400 to 500 m higher (*8*) during the LGM and early Holocene. Byrd core $\delta^{18}O$ data imply that ice elevations were ~500 m higher during the LGM (*9*). Here, we present new surface exposure ages from a lateral moraine band at Mount Waesche that directly date the most recent ice high stand in interior West Antarctica.

Mount Waesche is the southernmost volcano in the Executive Committee Range, a line of volcanoes that projects through the WAIS in Marie Byrd Land (Fig. 1). Regional ice flow is southward from a dome centered on the northern Executive Committee Range, where ice

[1]Massachusetts Institute of Technology/Woods Hole Oceanographic Institution Joint Program, MS 25, Clark 419, [2]Department of Marine Chemistry and Geochemistry, Woods Hole Oceanographic Institution, Woods Hole, MA 02543, USA. [3]Department of Geology, State University of New York at Cortland, Cortland, NY 13045, USA. [4]Institute for Quaternary Studies, [5]Department of Computer Science, University of Maine, Orono, ME 04469, USA. [6]Institute of Arctic and Alpine Research, University of Colorado, Boulder, CO 80309, USA. [7]Department of Earth and Environmental Science, University of Pennsylvania, Philadelphia, PA 19104–6316, USA.

*To whom correspondence should be addressed. E-mail: rackert@whoi.edu

elevations exceed 2200 m. WAIS elevations near Mount Waesche are ~2000 m. The summit caldera reaches 3200 m and is largely snow covered; small alpine glaciers terminate 400 m above the ice sheet surface. Extensive rock outcrops on the southwestern flank and an adjacent blue-ice area on the ice sheet indicate net ice ablation. Parasitic cones consisting of black vesicular lavas, cinders, and bombs overlie shield-building lava flows predominantly composed of alkali basalts and hawaiites. Limited K-Ar dating indicates that Mount Waesche is <1 million years old (*10*).

Two lateral moraines of the WAIS occur on the southwestern flank of the volcano (Fig. 2). An ice-cored lateral moraine adjacent to the present ice margin is composed of local tephra and pyroclastic debris. A higher lateral moraine band extends from the slope above the western end of the ice-cored moraine northwestward for ~3 km along the base of the volcano. The moraine varies in width from 150 to 300 m and generally increases in elevation to the northwest, rising irregularly to a maximum height of 120 m above the present ice margin. Like the ice-cored moraine, the lateral moraine band is composed of locally derived volcanic rocks. The rocks are primarily basalts containing plagioclase, olivine, and clinopyroxene. Clasts are subangular to angular and are typically <25 cm in length; no striated or glacially molded clasts were observed. We infer that the lateral moraines are composed of tephra and volcanic debris erupted onto the surface of the ice sheet (*11*). One difference between the ice-cored moraine and the higher lateral moraine band is that the latter is composed primarily of basalt fragments rather than pyroclastic debris. The greater abundance of basalt clasts on the higher moraine surface may have resulted from lavas that flowed out over the ice surface, along the ice margin, or from preferential weathering of the more erodible pyroclastic debris.

The uppermost surface of the distal section of the lateral moraine band occurs locally as a terrace 20 to 30 m wide, roughly parallel to the present ice margin. The relief is subdued and rarely exceeds 1 m. Below this part, the moraine surface consists of discontinuous subparallel ridges up to 5 m high and 100 to 200 m long that mark former ice margin positions. In general, the surface of the upper distal section of moraine is less hummocky than the lower proximal section, and the ridges are longer. Clast size is more uniform and smaller on the upper distal part, and fluting of clasts due to wind erosion (ventifaction) is most developed there. The change in character of the moraine surface from the upper distal to the more proximal parts of the lateral moraine band suggests that the moraine band is a complex feature and that the upper parts are older than the lower parts. Although there is not a clear morphologic break between the upper and lower parts, we divide the lateral moraine band into higher distal and lower proximal sections on the basis of the distribution of the surface exposure ages.

We collected samples for surface exposure dating along two transects across the lateral moraine band and from one isolated patch of lateral moraine in a similar setting (*12*). Clasts 10 to 20 cm in diameter were collected away from patterned ground and shattered boulders. The presence of pedogenic salts beneath the samples and ventifaction of the exposed surfaces were used as criteria for indicating the surface stability of the samples. In addition, samples were taken from in situ lava flow outcrops above the moraines and from a large pile of

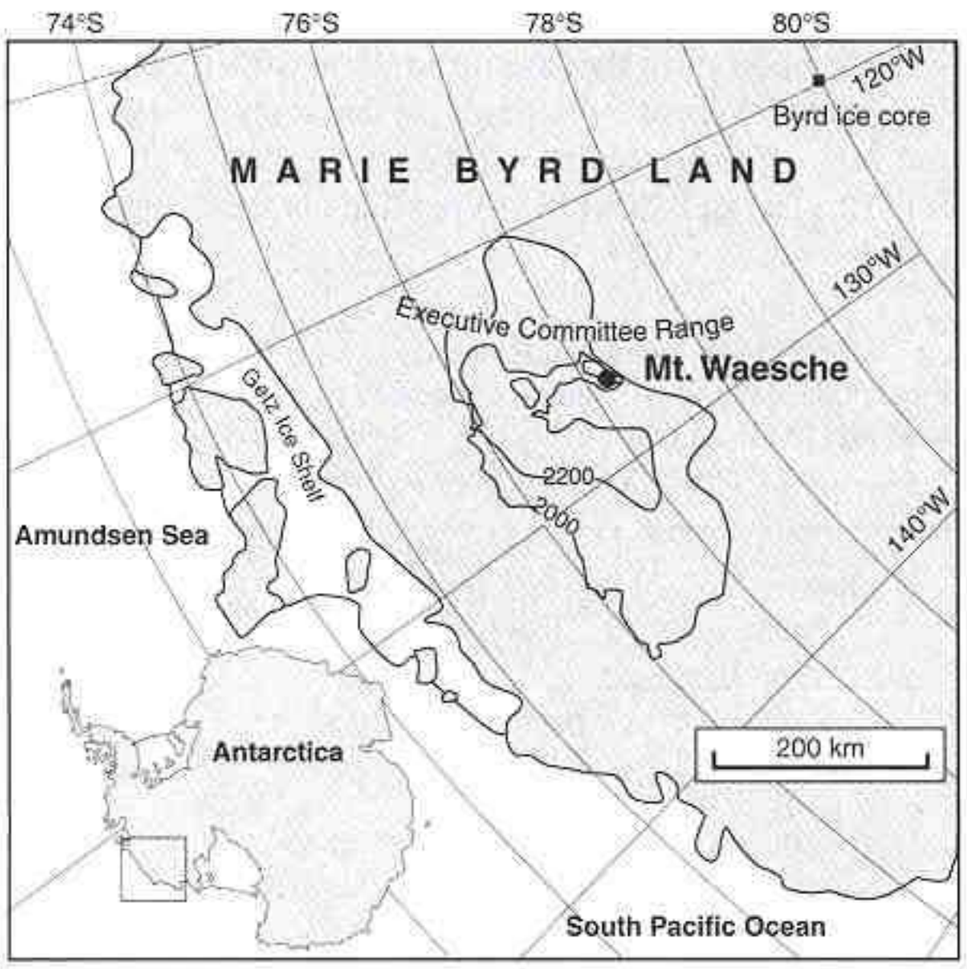

Fig. 1. Location map of Antarctica and Marie Byrd Land. Mount Waesche is a volcanic nunatak that projects through the WAIS near a dome of the ice sheet. Ice flows south around Mount Waesche to the Ross Ice Shelf. Moraines on Mount Waesche gauge past ice sheet elevations.

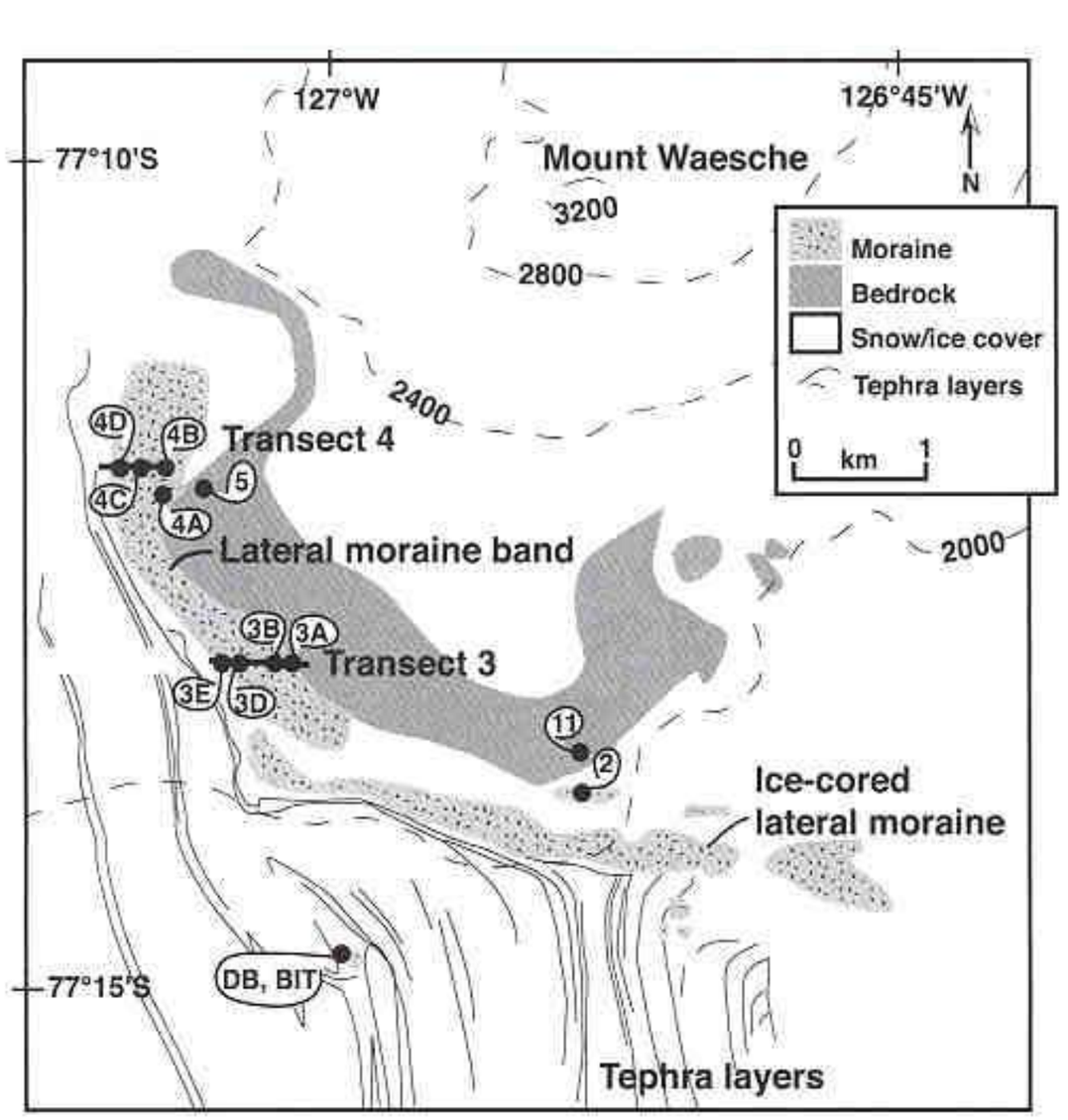

Fig. 2. Geologic sketch map of the southern flank of Mount Waesche. The map (*31*, *32*) shows the relation of englacial tephra layers to the lateral moraines. The ice-cored moraine is formed of tephra, which has been concentrated at the ice margin by ablation. Surface exposure sample locations are indicated (WA prefix omitted). Elevations are in meters.

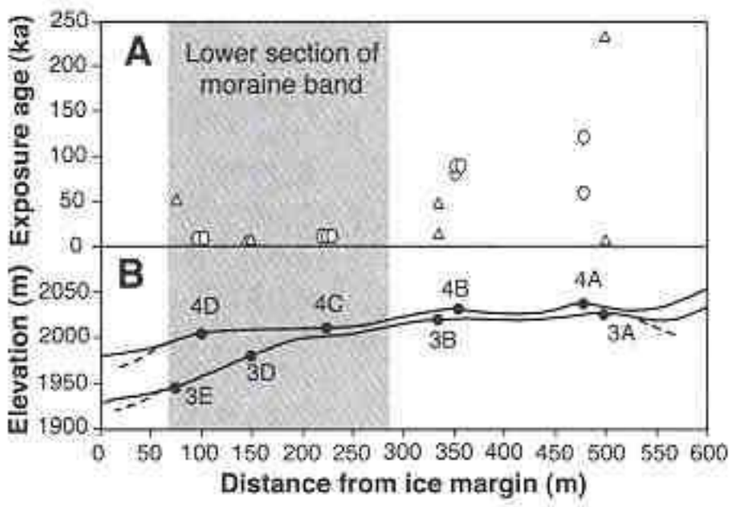

Fig. 3. (**A**) Exposure age of samples versus the distance along sample transects. Triangles are samples from transect 3; ovals are samples from transect 4. (**B**) Profiles and sample locations along transects 3 and 4. Dashed line represents the projected moraine surface beneath snow. The samples on the lower moraine band (shaded area) range from 6.2 to 10.6 ka; the best estimate is ~10 ka. The ages of samples from the upper section of the lateral moraine band are older and generally increase in exposure age with elevation and distance from the present ice margin.

coarse tephra on the ice sheet surface (Fig. 2).

Surface exposure dating was used to constrain the age of the lateral moraine band (*13*). The surface exposure dating technique relies on the buildup of cosmogenic nuclides (^{3}He, ^{21}Ne, ^{10}Be, ^{26}Al, and ^{36}Cl) in rocks exposed to cosmic rays at Earth's surface. The nuclides are formed primarily during spallation reactions between cosmic rays and major elements in the rock. A fundamental assumption is that accumulation of cosmogenic nuclides commenced at deposition on the moraine and has not been interrupted. In this case, the surface exposure age yields the age of moraine formation and the associated ice margin.

Erosion or shielding of a sample after deposition on a moraine would result in ages younger than the moraine. Exposure to cosmic rays before deposition would result in ages older than the moraine. Prior exposure in a surface exposure data set may be manifested by a scatter of ages older than a cluster of younger ages or ages substantially older than the age anticipated on the basis of other age constraints. At Mount Waesche, tephra and lava flows that erupted onto the ice sheet and were subsequently incorporated in glacial moraines are ideal for exposure dating, assuming that burial by ice is rapid and exposure after reemergence in the ablation zone is short.

Cosmogenic ^{3}He was measured in 24 separates of olivine or clinopyroxene (or both) from 19 samples (*14*). Four whole-rock ^{36}Cl measurements were made: two on porphyritic samples that also had ^{3}He measurements and two on aphanitic basalts in which ^{3}He measurements were not possible (Tables 1 and 2). In order to calculate accurate surface exposure ages from measured concentrations of cosmogenic nuclides, production rates calibrated on surfaces of known age must be scaled to the elevation and latitude of the sample (*15*). An additional complication in Antarctica is that anomalous low atmospheric pressure (thinner atmospheric depth) results in production rates that are up to 20 to 30% higher than those at 60° latitude. In this study, the high-latitude sea level production rates for ^{3}He (*16*) and ^{36}Cl (*17*) were scaled to the appropriate Antarctic altitude (*18*).

In general, the exposure ages increase with distance from and elevation above the ice margin (Fig. 3). The youngest samples, from tephra exposed in the ablation area, have exposure ages of <900 years ago and suggest that prior exposure is minimal. Two surface exposure ages [~360,000 years ago (~360 ka)] on lava flows are older than any sample from the moraine. The old lava flow ages indicate that erosion rates are low and suggest that mass wasting of material from the volcano slopes above has not supplied substantial amounts of debris to the lateral moraine band.

The paired ^{3}He and ^{36}Cl data can be used to evaluate erosion rates (Tables 1 and 2) (*19*, *20*). Because the ^{36}Cl production rate due to neutron capture on ^{35}Cl increases downward within the uppermost 10 cm of rock, erosion effectively increases the ^{36}Cl concentration at the surface. Low erosion rates [<5 mm/10^{3} years (ky)] can result in apparent ^{36}Cl surface exposure ages that are older than the true surface exposure age. The opposite effect occurs for ^{3}He, which is produced by spallation reactions. Concordant ages only occur within a narrow range of erosion rates that are similar to those determined from other Antarctic studies (0.5 to 1 mm/ky) (*21*). The younger samples constrain erosion rates to <0.5 mm/ky (WA-4C-1) and <3 mm/ky (WA-4D-1); the high Cl concentration of the older samples makes the ages very sensitive to erosion rates even as low as these. Comparison of ^{3}He and ^{36}Cl ages from location WA-4B suggests that erosion of that sample is negligible.

The surface exposure ages on the seven samples from four localities within the lower proximal section of the moraine band (Fig. 3)

Table 1. Helium-3 surface exposure data from Mount Waesche. SD, supraglacial debris; LMB, lower moraine band; UMB, upper moraine band; MP, moraine patch; LF, lava flows. Samples followed by "rep" are replicates; typically, the initial sample was not crushed, and the R/Ra crush value of the replicate was used for both samples. All samples were olivine separates, unless denoted by "cpx" (clinopyroxene).

Sample	Elevation (m)	R/Ra* ± 1σ crush	^{4}He ± 1σ (cm^{3} STP/g × 10^{-9})	R/Ra ± 1σ melt	Age† ± 1σ (ka)	Sample type
DB-94-1	1935	5.90 ± 0.04	47.3 ± 0.6	6.08 ± 0.1	0.4 ± 0.2	SD
BIT-252	1935	6.14 ± 0.10	2.14 ± 0.02	15.2 ± 0.3	0.9 ± 0.0	SD
WA-4D-1	2010	6.27 ± 0.08	44.7 ± 0.3	11.7 ± 0.1	10.6 ± 0.2	LMB
WA-4D-3 cpx	2010	5.62 ± 0.41	3.70 ± 0.09	44.0 ± 0.5	6.2 ± 0.2	LMB
WA-4C-2	2015	6.01 ± 0.12	32.8 ± 0.3	13.0 ± 0.1	10.1 ± 0.2	LMB
WA-4C-2 rep	2015	6.01 ± 0.12	3.79 ± 0.02	63.5 ± 0.5	9.6 ± 0.1	LMB
WA-4C-1	2015	6.13 ± 0.10	4.24 ± 0.04	60.6 ± 0.7	10.2 ± 0.2	LMB
WA-4B-1 cpx	2035	6.10 ± 0.05	31.8 ± 0.3	66.0 ± 0.3	83.2 ± 1.1	UMB
WA-4B-1	2035	6.10 ± 0.05	19.4 ± 0.2	104 ± 1	83.2 ± 1.0	UMB
WA-4B-1 cpx	2035	6.10 ± 0.05	9.13 ± 0.09	226 ± 1	87.8 ± 1.0	UMB
WA-4B-3	2035	6.05 ± 0.09	0.93 ± 0.01	2201 ± 30	87.8 ± 1.5	UMB
WA-4A-1	2040	5.42 ± 0.13	40.9 ± 0.4	40.9 ± 0.2	62.1 ± 0.9	UMB
WA-4A-1 rep	2040	5.42 ± 0.13	4.49 ± 0.09	328 ± 2	62.1 ± 1.3	UMB
WA-3E-1	1945	6.29 ± 0.12	2.27 ± 0.05	485 ± 4	49.5 ± 1.3	LMB
WA-3D-1	1985	5.30 ± 0.16	1.81 ± 0.02	120 ± 1	9.2 ± 0.2	LMB
WA-3D-2	1985	5.91 ± 0.15	1.70 ± 0.01	104 ± 1	7.4 ± 0.1	LMB
WA-3B-1	2025	6.03 ± 0.08	2.23 ± 0.03	174 ± 2	16.1 ± 0.3	UMB
WA-3B-2	2025	5.63 ± 0.06	5.45 ± 0.04	198 ± 1	47.0 ± 0.5	UMB
WA-3B-2 cpx	2025	6.08 ± 0.19	6.37 ± 0.07	169 ± 1	46.5 ± 0.7	UMB
WA-3A-1	2035	7.22 ± 0.18	4.49 ± 0.04	1217 ± 5	233 ± 2	UMB
WA-3A-2 cpx	2035	5.90 ± 0.05	3.41 ± 0.03	80.4 ± 0.6	10.9 ± 0.1	UMB
WA-3A-2	2035	5.89 ± 0.12	10.3 ± 0.1	28.1 ± 0.4	9.8 ± 0.2	UMB
WA-2-1	1975	6.38 ± 0.05	35.1 ± 0.4	94.5 ± 0.4	140.0 ± 2	MP
WA-2-1	1975	6.38 ± 0.05	6.64 ± 0.06	470 ± 2	139.3 ± 1	MP
WA-5-1	2055	6.82 ± 0.07	22.8 ± 0.2	376 ± 2	360 ± 4.1	LF
WA-5-1 rep	2055	6.64 ± 0.04	6.60 ± 0.12	1290 ± 4	362 ± 7	LF
WA-5-1 cpx	2055	6.64 ± 0.06	6.09 ± 0.06	1343 ± 4	348 ± 4	LF
WA-11-1	2055	6.67 ± 0.05	3.32 ± 0.04	2547 ± 14	360 ± 5	LF

*R/Ra is the ^{3}He/^{4}He ratio in relation to the atmospheric ratio (1.384 × 10^{-6}). R/Ra crush is the ratio of the inherited (magmatic) He component. The mean R/Ra crush (6.11 ± 0.46, n = 21) characterizes the mantle source beneath the Executive Committee Range. Helium-4 is the gas released on melting in vacuo. †The surface exposure ages were calculated with a ^{3}He production rate of 121 ± 4 atoms/g per year (high-latitude sea level) (*16*). The production rate, higher than that previously published, results from an updated conversion from ^{14}C years before the present to calendar years (*33*). Scaling to Antarctic altitudes was done following Stone (*18*). Uncertainties are propagated analytical uncertainties only. Scaling and production rate uncertainties are <10%.

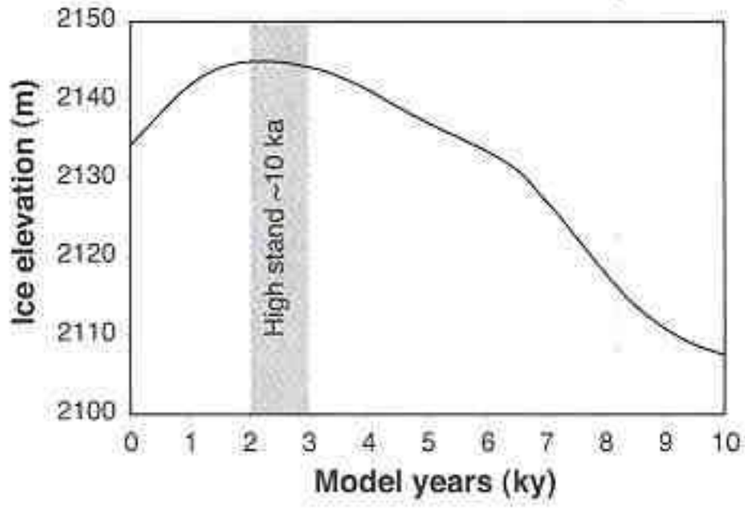

Fig. 4. Elevation changes at Mount Waesche generated by the ice sheet model, described in text (*25*), tuned to the existing chronology from the Ross Embayment (*4*). Model years are time since the start of deglaciation. Maximum ice elevations occur over 2000 years after the start of deglaciation in the Ross Sea (14 to 11 ka). The model elevations are for the 20 km by 20 km grid unit containing Mount Waesche and are not necessarily the elevations at the sample sites; the relative elevation change is more robust than the absolute elevations. The timing and magnitude of ice elevation changes at Mount Waesche are similar to the glacial geologic evidence.

show, with one exception, similar ages. The sample nearest the ice margin (WA-3E-1) has an anomalously old age (~50 ka), suggesting prior exposure, and was rejected. The mean of the other six samples is 9.0 ± 1.8 ka. There does not appear to be a relation between surface exposure age and position on the lower part of the moraine. The oldest and youngest samples were collected from the same location, so the younger samples do not simply represent progressive lowering of the ice margin. Rather, the samples with slightly younger ages probably reflect postdepositional exhumation by frost action or erosion by boulder shattering (*22*). If the two younger samples are removed, the four remaining samples form a tight cluster of ages; the mean of these samples is 10.0 ± 0.6 ka and may be a better age estimate for the lower part of the moraine. The uncertainty in the mean is similar to the 2σ analytical uncertainty and the exposure ages of the samples from the ice surface. In either case, the mean ages indicate that the interior of the WAIS was up to 45 m thicker at ~10 ka.

The exposure ages of samples from the transects across the upper distal part of the moraine band and from the isolated moraine outcrop (Fig. 2) vary from 10.8 to 231 ka along the moraine (Fig. 3). Because nonconcordant exposure ages occur at most sample locations and the ages do not cluster around some value (as is the case on the proximal part of the moraine), we do not assign an age to the upper section of the moraine band. The older surface exposure ages are consistent with observations of surface morphology that indicate an older age for at least some parts of the upper distal section of the moraine band. The scatter of ages may reflect breakup of boulders after deposition, exhumation by frost action, prior exposure of debris derived from the volcano slopes, or record earlier WAIS high stand events. Cold-based ice can override surfaces without causing substantial disturbance. The surface exposure age of sample WA-3A-2, which falls within the age range of samples from the lower part of the moraine band, may indicate that WAIS elevations were up to 85 m above the present ice surface during the last ice sheet high stand.

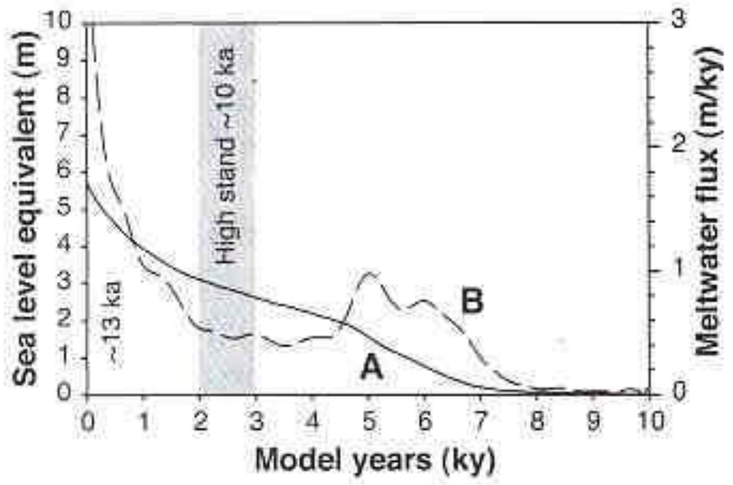

Fig. 5. Sea level equivalent and meltwater flux from the Ross Sea sector of the WAIS during deglaciation. Model years are time since the start of deglaciation. Ice volume is represented by line A. Only ~3 m of sea level equivalent remain at ~10 ka. Meltwater flux is represented by dashed line B. The maximum Holocene values are ~1 /ky and occur during the middle Holocene.

The $\delta^{18}O$ record from the Byrd ice core indicates that the age obtained for the most recent ice sheet high stand at Mount Waesche falls near the end of a 3000-year period of strong warming in West Antarctica that culminated at the start of the Holocene (*23*). Grounding line retreat of the WAIS was well underway by ~11 ka (*4*), and ice retreat in the McMurdo Sound region began by 14 ka (*2*). Apparently, maximum ice elevations around Mount Waesche occurred several thousand years after the maximum ice extent in the Ross Sea. This conclusion is consistent with results from a quasi–three-dimensional ice sheet model of the WAIS tuned to fit the available chronology of ice advance and deglaciation from the Ross Embayment. The model provides a finite element solution of a two-dimensional (map-plane) time-dependent mass continuity equation that integrates ice flow in a vertical column of ice (*24, 25*). In the model, the difference between the maximum elevation and that at the end of the model run at Mount Waesche is ~40 m (Fig. 4).

Ice sheet growth and decay in this model is driven solely by changes in calving rates, which, to first order, simulate the effects of sea level change on the ice sheet. This simple approach is justified by results from more complex three-dimensional time-dependent thermomechanical ice sheet models, which suggest that eustatic sea level is the primary control on the configuration of the Antarctic Ice Sheet (*26*). In the model, the WAIS does not have sufficient time to equilibrate with its extended grounding line position during the LGM, consistent with other models (*27*). As a consequence, interior elevations continue to thicken during grounding line retreat until the initial wave of thinning reaches the interior of the ice sheet.

The similarity of the model results with the glacial geologic evidence at Mount Waesche may be serendipitous: If a factor-of-2 change in snow accumulation rates in the WAIS interior between the LGM and the Holocene, as indicated by ice core data (*28*), is included in the model, maximum elevations are lower and occur several thousand years later than what is observed. This implies that the current version of the model may overestimate the ice-dynamics response time to changes in boundary conditions, likely because of unrealistic simulation of ice stream dynamics (*25*). However, with accumulation held constant, the model produces an elevation history for interior West Antarctica that is in excellent agreement with elevation changes inferred for the Byrd ice core (*8, 25*).

The model time scale (years after the start of grounding line retreat) can be converted to calendar years by pinning the maximum ice elevations predicted at Mount Waesche to the age of the lower part of the moraine band (Fig. 4). The model results may then be used to constrain the timing and magnitude of Holocene ice volume changes in the Ross Sea sector of the WAIS. In the model, most ice is lost early (Fig. 5, line A). By ~10 ka (3000 model years), only ~3 m of excess sea level equivalent remains. Because the model accurately predicts ice levels at Mount Waesche, it is unlikely that the interior WAIS volume is substantially underestimated. Most of the remaining ice is released during a short pulse in the early Holocene (Fig. 5, line B).

These results have implications for the contribution of the WAIS to eustatic sea level rise during the last termination. The Antarctic Ice Sheet, and the WAIS in particular, has been suggested as the source of the two meltwater pulses responsible for the abrupt rises in sea level recorded in the Barbados coral record (*29*). The later of these two events, meltwater pulse 1B, refers to an ~28 m of sea level rise in 1000 years at 11 ka. The ice mass responsible for meltwater pulse 1B is located in Antarctica in global models of deglaciation that are based on geophysical predictions of postglacial relative sea level change (ICE-3G and ICE-4G) (*30*). Our results indicate that there is insufficient ice remaining in the WAIS for it to be the

Table 2. Chlorine-36 data from Mount Waesche. Σ is the macroscopic absorption cross section of the rock. Exposure ages were calculated with ^{36}Cl spallation production rates (P) from (*17*): P_{Ca} = 73.3 ± 4.9 atoms/g of Ca per year, P_K = 154 ± 10 atoms/g of K per year. The thermal neutron activation production rate was calculated after (*19*). Exposure ages were calculated for erosion rates of 0 (e = 0) and 1 mm/ky (e = 1). Ages calculated with low erosion rates are younger because the production of ^{36}Cl increases with depth. Chlorine-36 was measured in AgCl targets at the Purdue Rare Isotope Measurement Laboratory (Purdue University, West Lafayette, IN); exposure ages were calculated with the CHLOE program (*34*). Combined analytical and systematic uncertainties are <15%; ppm, parts per million.

Sample	K_2O (%)	CaO (%)	Cl (ppm)	Σ (cm^2/kg)	$^{36}Cl/Cl$ (10^{-15})	Exposure age (ka)	
						e = 0	e = 1
WA-4A-2	2.14	6.10	1007	14.1	1365	130	96.1
WA-4B-2	2.10	6.16	761	14.3	1038	88.1	69.3
WA-4C-1	0.78	10.50	201	14.0	254	10.9	10.5
WA-4D-1	0.80	10.50	172	13.6	245	9.4	9.2

primary source of meltwater pulse 1B. This conclusion is not strongly dependent on the ice sheet model.

References and Notes

1. J. H. Mercer, *Geol. Soc. Am. Bull.* **79**, 471 (1968); J. G. Bockheim, S. C. Wilson, G. H. Denton, *Quat. Res.* **31**, 229 (1989); G. H. Denton, J. G. Bockheim, S. C. Wilson, J. E. Leide, B. G. Anderson, *ibid.*, p. 189.
2. G. H. Denton, J. G. Bockheim, S. C. Wilson, M. Stuiver, *Quat. Res.* **31**, 151 (1989); E. J. Brook, M. D. Kurz, R. P. Ackert Jr., G. Raisbeck, F. Yiou, *Earth Planet. Sci. Lett.* **131**, 41 (1995); B. L. Hall and G. H. Denton, *Geogr. Ann.*, in press.
3. J. B. Anderson, S. S. Shipp, L. R. Bartek, D. E. Reid, in *Contributions to Antarctic Research III*, vol. 57 of *Antarctic Research Series*, D. H. Elliot, Ed. (American Geophysical Union, Washington, DC, 1992), pp. 39–62; S. Shipp, J. B. Anderson, E. W. Domack, *Geol. Soc. Am. Bull.*, in press.
4. K. J. Licht, A. E. Jennings, J. T. Andrews, K. M. Williams, *Geology* **24**, 223 (1996); K. J. Licht, N. W. Dunbar, J. T. Andrews, A. E. Jennings, *Geol. Soc. Am. Bull.* **111**, 91 (1999); E. W. Domack, E. A. Jacobson, S. Shipp, J. B. Anderson, *ibid.*, in press.
5. G. H. Denton, M. L. Prentice, L. H. Burkle, in *The Geology of Antarctica*, R. J. Tingey, Ed. (Clarendon, Oxford, 1991), pp. 365–419.
6. P. Martinerie, D. Raynaud, D. M. Etheridge, J. Barnola, D. Mazaudier, *Earth Planet. Sci. Lett.* **112**, 1 (1992).
7. D. Raynaud and B. Lebel, *Nature* **281**, 289 (1979); D. Raynaud and I. M. Whillans, *Ann. Glaciol.* **3**, 269 (1982).
8. D. Jenssen, in *The Climate Record in Polar Ice Sheets*, G. d. Q. Robin, Ed. (Cambridge Univ. Press, London, 1983), pp. 138–144.
9. P. Grootes and M. Stuiver, *Quat. Res.* **26**, 49 (1986).
10. W. LeMasurier and Y. Kawachi, in *Volcanoes of the Antarctic Plate and Southern Oceans*, vol. 48 of *Antarctic Research Series*, W. LeMasurier and J. W. Thompson, Eds. (American Geophysical Union, Washington, DC, 1990), pp. 208–211; W. LeMasurier and D. C. Rex, *J. Geophys. Res.* **94**, 7223 (1989).
11. Tephra layers erupted onto the surface of the ice sheet are exposed in the ice sheet ablation area on the southwest side of Mount Waesche. The layers include locally derived pyroclastic debris and basalt clasts up to 4 m thick (*31*). Individual tephra layers can be traced to the ice-cored moraine, demonstrating that englacial tephra is the source material for the ice-cored moraine.
12. Sample locations were recorded with handheld global positioning systems (GPSs); sample elevations were determined by altimeter in relation to a base camp on the ice sheet. Relative uncertainties in elevation between sample sites are estimated to be ±5 m. The relative elevations were tied to geodetic altitude by differential GPSs (±20 m) at several locations.
13. F. M. Phillips *et al.*, *Science* **274**, 749 (1996); J. C. Gosse, J. Klein, E. B. Evenson, B. Lawn, R. Middleton, *ibid.* **268**, 1329 (1995); E. J. Brook *et al.*, *Quat. Res.* **39**, 11 (1993).
14. M. D. Kurz, *Geochim. Cosmochim. Acta* **50**, 2855 (1986). The inherited (mantle-derived) $^3He/^4He$ ratio was determined by crushing the mineral separates in vacuo, which selectively released gases held in fluid and melt inclusions. The cosmogenic ^3He component is calculated by subtracting the initial ^3He from that released by fusion of the sample powders in vacuo.
15. D. Lal, *Earth Planet. Sci. Lett.* **104**, 424 (1991).
16. T. E. Cerling and H. Craig, *Geochim. Cosmochim. Acta* **58**, 349 (1994).
17. F. M. Phillips, M. G. Zreda, M. R. Flinsch, *Geophys. Res. Lett.* **23**, 949 (1996).
18. J. O. Stone, personal communication.
19. B. Liu, F. M. Phillips, J. T. Fabryka-Martin, M. M. Fowler, W. D. Stone, *Water Resour. Res.* **30**, 3115 (1994).
20. F. M. Phillips *et al.*, *Geol. Soc. Am. Bull.* **109**, 1453 (1997).
21. E. T. Brown *et al.*, *Geochim. Cosmochim. Acta* **55**, 2269 (1991); K. Nishiizumi, C. P. Kohl, J. R. Arnold, J. Klein, D. Fink, *Earth Planet. Sci. Lett.* **104**, 440 (1991).
22. Although areas of active cryoturbation were avoided when sampling, greater activity in the past is difficult to rule out. Basalt boulders derived from lava flows tend to be highly jointed and disintegrate relatively rapidly along these joint surfaces. Subsequent (measured) erosion of the fragments is slow and primarily by wind.
23. T. Sowers and M. Bender, *Science* **269**, 210 (1995).
24. J. L. Fastook and M. Prentice, *J. Glaciol.* **40**, 167 (1994).
25. E. J. Steig *et al.*, in preparation.
26. P. Huybrechts, *Clim. Dyn.* **5**, 79 (1990).
27. ———, *Ann. Glaciol.* **5**, 115 (1990).
28. E. J. Steig, *ibid.* **25**, 418 (1997).
29. R. G. Fairbanks, *Nature* **342**, 637 (1989).
30. A. M. Tushingham and W. R. Peltier, *J. Geophys. Res.* **96**, 4497 (1991); W. R. Peltier, *Science* **265**, 195 (1994).
31. N. W. Dunbar, R. P. Esser, W. C. McIntosh, *Antarct. J. U.S.*, in press.
32. H. W. Borns Jr., C. Dorion, P. E. Calkin, G. C. Wiles, D. Barclay, *ibid.* **XXX**, 100 (1995).
33. M. Stuiver and P. J. Reimer, *Radiocarbon* **25**, 215 (1993).
34. F. M. Phillips and M. A. Plummer, *ibid.* **38**, 98 (1996).

35. This research was supported by NSF grants OPP 93-18872 (H.W.B. and P.E.C.), OPP 94-18333, and EAR 96-14561 (M.D.K.). The authors thank S. Murphy for assistance in sample preparation, D. Lott and J. Curtice for maintaining the mass spectrometer, and L. Woodward for drafting figures. N. Dunbar provided samples, differential GPS elevations, and valuable discussion. G. Wiles, C. Dorion, and T. Redfield assisted in the fieldwork. This is Woods Hole Oceanographic Institution contribution 10026.

16 July 1999; accepted 9 September 1999

Past and Future Grounding-Line Retreat of the West Antarctic Ice Sheet

H. Conway,[1] B. L. Hall,[2,3] G. H. Denton,[2] A. M. Gades,[1] E. D. Waddington[1]

The history of deglaciation of the West Antarctic Ice Sheet (WAIS) gives clues about its future. Southward grounding-line migration was dated past three locations in the Ross Sea Embayment. Results indicate that most recession occurred during the middle to late Holocene in the absence of substantial sea level or climate forcing. Current grounding-line retreat may reflect ongoing ice recession that has been under way since the early Holocene. If so, the WAIS could continue to retreat even in the absence of further external forcing.

The grounding line of the WAIS has retreated nearly 1300 km since the Last Glacial Maximum (LGM) about 20,000 years before present (yr B.P.), when grounded ice in the Ross Sea Embayment extended almost to Coulman Island (*1–3*) (Fig. 1). Complete collapse of the WAIS would cause sea level to rise 5 to 6 m. Estimates of the present stability of the WAIS are hampered by uncertainties in the overall mass balance (*4*) and uncertainties concerning the dynamic response of the ice sheet to changes in sea level or climate. It is thought that it would take ~10^4 years for the WAIS to reach equilibrium after a perturbation (*5*), but accurate assessment is difficult because the dynamics of the present ice sheet is dominated by ice streams. Fast-flowing ice streams evacuate inland ice rapidly, but field evidence indicates that abrupt changes from fast to slow flow have occurred in the past (*6*). We look to the deglacial history of the WAIS for clues about its future. Below we present dates from three locations, southern Scott Coast, Hatherton Coast, and Roosevelt Island (Fig. 1), that resolve the Holocene deglaciation of the Ross Sea Embayment.

At the LGM, outlet glaciers that flowed through the Transantarctic Mountains and across the coast thickened substantially where they merged with grounded ice filling the Ross Sea Embayment. Only along the southern Scott Coast adjacent to McMurdo Sound, 450 km south of Coulman Island, did the Ross Sea ice sheet terminate on land in the mouths of ice-free Taylor Valley and dry valleys fronting the Royal Society Range (Fig. 1). This peculiar situation arose because only here did East Antarctic ice and alpine glaciers terminate well inland, leaving the coast susceptible to incursions of landward-flowing grounded ice at the LGM. Over 200 ^{14}C dates of lacustrine algae from proglacial lakes (*3*, *7*, *8*), dammed in these valleys by grounded ice, show that the Ross Sea ice sheet was close to its LGM position from at least 27,820 to 12,880 calendar yr B.P. (*9*).

The grounding line was still north of McMurdo Sound 9420 yr B.P.; this date corresponds to the youngest delta of a proglacial lake dammed in Taylor Valley by grounded Ross Sea ice (*3*, *8*). Two thousand years later, the McMurdo Sound region was free of grounded ice, based on two lines of evidence. First, molluscs recolonized the area after the

[1]Geophysics Program, University of Washington, Seattle, WA 98195, USA. [2]Institute for Quaternary Studies and Department of Geological Sciences, University of Maine, Orono, ME 04469, USA. [3]Department of Geology and Geophysics, Woods Hole Oceanographic Institution, Woods Hole, MA 02543, USA.